

1 Statistical and neural network assessment of the climatology of 2 fog and mist at Pula airport in Croatia

3
4 Marko Zoldoš^{*1,2}, Tomislav Džoić^{*3}, Jadran Jurković², Frano Matic⁴, Sandra Jambrošić², Ivan
5 Ljuština², Maja Telišman Prtenjak⁵

6
7 ¹Risk Management Division, Erste & Steiermärkische Bank d.d., Rijeka 51000, Croatia (ORCID: 0009-0005-1117-
8 5716)

9 ²Aviation Meteorology department, Croatia Control Ltd., Velika Gorica 10410, Croatia

10 ³Laboratory of Physical Oceanography, Institute of Oceanography and Fisheries, Split 21000, Croatia (ORCID: 0000-
11 0001-9585-8779)

12 ⁴University Department ~~Department~~ of Marine Studies, University of Split, Split 21000, Croatia (ORCID: 0000-
13 0003-0392-4172)

14 ⁵Department of Geophysics, Faculty of Science, University of Zagreb, Zagreb 10000, Croatia (ORCID: 0000-0002-
15 4941-8278)

16
17
18 **Leading author: Marko Zoldoš, correspondence to: Tomislav Džoić (dzoic@izor.hr)*
19
20

21 **Abstract.** A study was conducted on the climatological characteristics of fog and mist at Pula Airport in the
22 northeastern Adriatic, using statistical and machine learning approaches. The study utilized meteorological data from
23 Pula Airport, along with satellite sea surface temperature (SST) data from two coastal areas west and east of the
24 airport, to gain insights into the influence of sea temperature on fog formation. To identify weather patterns associated
25 with the occurrence of fog and mist, wind and mean sea-level pressure (MSLP) data from the ERA5 reanalysis were
26 analyzed using Growing Neural Gas (GNG), a machine learning method. A notable finding was a declining trend in
27 the frequency of fog and mist at the airport, which can be linked to the results of the GNG analysis of the ERA5 data.
28 This analysis showed a decrease in synoptic patterns favorable for fog and mist. Fog occurs mainly between October
29 and March and is primarily associated with weak westerly and northwesterly winds. Additionally, fog is more likely
30 to occur when the sea surface temperature is higher than the air temperature. Mist has similar characteristics to fog,
31 although it is more likely to occur with easterly winds.
32
33
34
35
36
37
38

Commented [MZ1]: Added missing ORCID and corrected the institution's name

39 **1 Introduction**

40 According to the World Meteorological Organization (WMO), fog is the suspension of very small water droplets or
41 ice crystals in the atmosphere, reducing visibility on the Earth's surface to less than 1 km (WMO, 1966). The formation
42 of these water droplets and ice crystals is influenced by factors such as cooling, increased humidity, and the mixing
43 of air masses with different temperatures (Gultepe et al., 2007). Mist, a related phenomenon, occurs when horizontal
44 visibility at the surface is between 1 and 10 km, with aviation meteorology specifically defining mist as conditions
45 where visibility is between 1 and 5 km. Fog is a unique atmospheric phenomenon confined to the atmospheric
46 boundary layer (ABL), the lowest part of the atmosphere, and its characteristics are influenced by the Earth's surface.
47 The formation and dissipation of fog are impacted by synoptic and mesoscale conditions, as well as surface features
48 such as moisture sources (e.g., oceans, lakes, rivers), vegetation, orography, urban areas, and sea currents.

49
50 This study examines fog occurrence over an extended period at Pula Airport, located in the coastal region of Croatia
51 in the northeastern Adriatic (Figure 1). The Adriatic Sea is a large semi-enclosed sea separating the Apennine
52 Peninsula from the Balkans. It is the northernmost arm of the Mediterranean Sea, extending from the Strait of Otranto
53 (where it connects to the Ionian Sea and the rest of the Mediterranean) to the northwest, toward the Po Valley and the
54 Istria Peninsula. This region frequently experiences marine fog due to synoptic-scale effects that can trigger
55 subsidence within the boundary layer, which causes stratus clouds to descend to the surface. Similar marine fog events
56 have been studied in the northwestern Pacific and Atlantic Oceans (e.g., Koraćin et al., 2001; Koraćin and Dorman,
57 2017). In the Adriatic, fog typically occurs between September and May, often disrupting sea transport and port
58 operations (Popović et al., 2014). Fog also significantly affects air traffic at airports, where it can cause significant
59 flight delays due to poor visibility and low cloud ceilings. These delays result in substantial financial losses for airlines,
60 underscoring the need for accurate fog forecasting. For example, dense fog at New Delhi Airport in India caused losses
61 of approximately 3.9 million U.S. dollars between 2011 and 2016 (Kulkarni et al., 2019). Improved fog forecasting
62 could mitigate such losses, as illustrated by Allan (2001), who estimated that better forecasts for low-visibility events
63 at three New York City airports could save up to \$240,000 per event.

64
65 These factors highlight the critical role of fog research in advancing forecasting capabilities. Despite its importance,
66 the study of fog remains an area of atmospheric science where our understanding is limited, both over land (Gultepe
67 et al., 2007) and ocean (Koraćin and Dorman, 2017). Fog formation involves a complex interaction of processes
68 ranging from synoptic to microscale levels. The typical size of fog condensation nuclei is around $0.1 \mu\text{m}$ (10^{-5} cm),
69 while the synoptic-scale processes that contribute to fog development occur on a scale of 10^8 cm or more, making the
70 ratio of interacting length scales about 10^{13} . Fully understanding fog formation involves various elements, including
71 large-scale synoptics (Belo-Pereira and Santos, 2016), characteristics of the surface and radiation exchange
72 (Duynkerke, 1991), microphysics (Gultepe and Milbrandt, 2007; Wang et al., 2019), climatology (Stolaki et al., 2009;
73 Veljović et al., 2015), relationships with turbulence intensity (Ju et al., 2020), presence of aerosol (Oztaner and
74 Yilmaz, 2013), and more. The complicated interplay of meteorological parameters that determine whether fog forms
75 or not poses a substantial challenge for accurate fog forecasting (Bergot and Koraćin, 2021). In addition to local factors

76 influencing fog and mist formation, the impact of global warming and climate change cannot be overlooked. These
77 global phenomena have been linked to a reduction in the number of days with fog and mist (Kawai et al., 2016; Klemm
78 and Lin, 2016). Considering that fog occurrence in the eastern Adriatic has been studied infrequently, with the most
79 recent research conducted over 50 years ago (Stipaničić, 1972), there is a need for updated insights.

80
81 This study analyzes the climatological characteristics of fog at Pula Airport, Croatia, with a focus on understanding
82 the general patterns of fog initiation and dissipation. The primary objective is to provide detailed statistical analyses
83 to help understand the local and dynamic processes leading to fog development. A secondary objective is to assess the
84 influence of sea surface temperature (SST) in the vicinity of the study area on the frequency and intensity of advective
85 fog. SST has been shown to significantly impact the accuracy of numerical weather prediction (NWP) models (Huang
86 et al., 2022). To achieve these goals, the Growing Neural Gas Network (GNG), an unsupervised machine learning
87 algorithm within artificial neural networks (Martinetz and Schulten, 1991), was applied. This method classifies
88 synoptic conditions that prevail before and during the occurrence of fog at Pula into distinct weather patterns, and
89 identifies those that favor fog development. The results of this research could aid local forecasters in improving fog
90 prediction by accounting for specific terrain and coastline features, as well as synoptic and local influences
91 (particularly SST), thereby closing a gap in scientific knowledge about fog characteristics in this part of the
92 Mediterranean.

93 **2 Location, data and methods**

94 **2.1 Location**

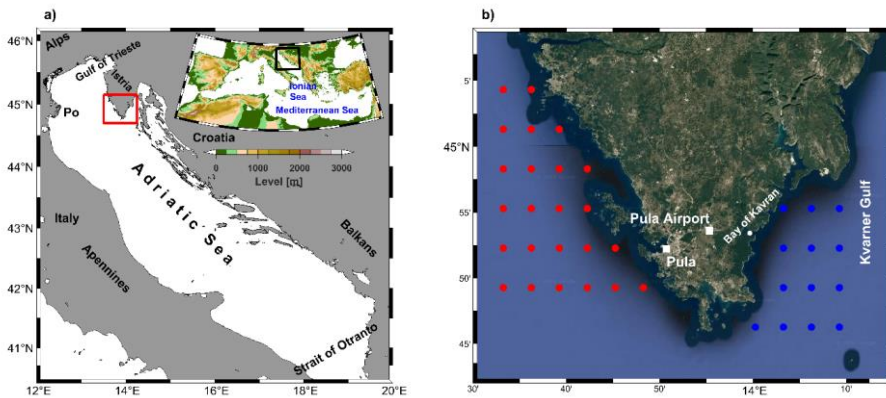
95 Pula Airport, located approximately 6 km ENE of the coastal city of Pula in western Croatia (Figure 1b), serves as the
96 region's international airport. Its geographical coordinates are 44°53'37" N and 13°55'20" E, with an elevation of 84
97 meters above mean sea level (AMSL). In 2023, the airport served 413,439 passengers, ranking as the fifth busiest
98 airport in Croatia by passenger traffic (source: <https://podaci.dzs.hr/2023/en/58556>). The airport is situated at the
99 southern tip of the Istrian Peninsula—the largest peninsula in the Adriatic Sea—positioned between the Gulf of Trieste
100 to the northwest and the Kvarner Gulf to the east. The climate of Istria is influenced by Alpine and Dinaric Alps
101 mountain ranges and the Mediterranean Sea. Winters in Istria are typically mild and wet, while summers are hot and
102 humid. The interior of Istria experiences a more continental climate, while the coastal area is significantly influenced
103 by the Adriatic Sea. Recent research has analyzed bioclimatic parameters, highlighting these climatic boundaries
104 across the peninsula (e.g., Omazić et al., 2020).

105
106 Two weather patterns are primarily associated with fog in Pula. The first involves a westerly to northwesterly flow
107 that advects moist air under anticyclonic conditions. In these cases, advection can occur over a broad geographical
108 area. Fog is often advected from the Po Valley in northern Italy, where it is a frequent phenomenon during the fall-
109 winter season (Mariani, 2009), across the northern Adriatic to the Istrian coast. Under such conditions, fog can persist
110 for days across the affected region (Bendix, 1994). For example, Linate Airport in Milan, Italy, historically

111 experienced the highest number of annual closures due to fog among European airports (Mariani, 2009). While
 112 advective fog is less common in the northwestern Adriatic, it still frequently occurs on the western coast of Istria
 113 (Tešić and Brozinčević, 1974), which is climatologically the foggiest area of the eastern Adriatic (Stipaničić, 1972).
 114 The second weather pattern associated with fog in Pula involves an easterly to southeasterly flow during a weakening
 115 anticyclone, often advecting moist air from the southeast. These patterns are linked to the broader atmospheric
 116 circulation over the Adriatic Sea, which is shaped by four dominant wind regimes. The northeasterly bora and the
 117 southeasterly sirocco winds, both common in the colder months, are influenced by regional synoptic systems. In
 118 contrast, during warmer months, sea/land breezes and, to a lesser extent, the Etesian wind, become more prominent.
 119 The wind regime strongly influences changes in wind direction at Pula Airport (e.g., Pandžić and Likso, 2005; Prtenjak
 120 and Grisogono, 2007; Prtenjak et al., 2010; Belušić et al., 2018).

121
 122 The terrain surrounding the airport is predominantly flat, covered with grassland and small forested areas. There are
 123 no significant hills or mountains nearby that would notably influence the local weather or climate. The central part of
 124 the airport, along with its southern surroundings, lies within a very shallow basin, which is prone to nighttime
 125 inversions during calm wind conditions and clear skies (as reported by local forecasters). The proximity of the sea
 126 exerts a substantial influence on the airport's weather. Pula Bay is located 6 km to the west-southwest, while the open
 127 waters of the northern Adriatic Sea are just 10 km away. To the east, the open sea is 7 km away, with the small Bay
 128 of Kavran situated just 5 km from Pula Airport. These geographical factors contribute to the significant marine
 129 influence on the weather at Pula Airport, even though the airport itself is not directly on the coast.

130
 131



132
 133 **Figure 1. a) Map of the bathymetry of the Adriatic Sea, with the black square marking the Adriatic Sea area. The red**
 134 **rectangle on the map marks the immediate surroundings of Pula Airport (b) (© Google Maps 2024). The important localities**
 135 **are marked with white squares, while blue and red dots mark the eastern and western grid points from which the satellite**
 136 **SST values were extracted. The wider area of the Mediterranean Sea corresponds to the area of the ERA5 reanalysis.**

137 **2.2 Data and methods**

138 The dataset used for this study includes half-hourly METAR reports and three-hourly SYNOP reports from the
139 meteorological station at Pula Airport. METAR (METeorological Aerodrome Report) is a coded report describing
140 weather conditions at the airport in a manner standardized for aviation. SYNOP (Surface Synoptic Observations) is a
141 coded report describing weather conditions at a meteorological station. An airport meteorological station sends both
142 SYNOP and METAR reports. The meteorological variables considered are wind speed and direction, temperature at
143 2 meters above ground, dew point temperature, relative humidity, surface pressure, cloud cover, and horizontal
144 visibility. These variables are reported by both station observers and automatic instruments. The dataset spans a 20-
145 year period from January 1, 2001, to December 31, 2020, with all measurements recorded at the airport's
146 meteorological station. Runway 27, the primary operational runway, is equipped for Category I operations. This allows
147 for takeoff and landing under low visibility conditions with a Runway Visual Range (RVR) of up to 550 meters or a
148 ceiling height of 200 feet (approximately 60 meters). This capability underscores the operational challenges posed by
149 fog: visibility below 550 meters prohibits aircraft landings and takeoffs.

150
151 In addition to the airport data, daily sea surface temperature (SST) measurements from the Pula Bay oceanographic
152 station were included. These SST values, recorded at 07:00, 14:00, and 21:00 local time from January 1, 2001, to
153 December 31, 2020, were supplemented with reprocessed satellite SST data from the Copernicus Marine Data Store
154 (<https://data.marine.copernicus.eu/>). This gap-free dataset, which has been optimally interpolated with a grid
155 resolution of 0.05° (Merchant et al., 2019), provides a comprehensive view of sea surface temperatures. Two coastal
156 areas were selected for analysis: one to the west of the airport, encompassing the open Adriatic Sea, and the other to
157 the east, covering the Kvarner Gulf (Figure 1). These regions were chosen to calculate the average spatial SST for a
158 given day and evaluate their influence on fog formation. The selected areas are representative of the nearshore waters
159 where the prevailing winds most frequently originate.

160
161 To identify the synoptic wind and pressure fields associated with fog occurrence at Pula Airport and across the
162 Mediterranean region, 10-meter wind and mean sea-level pressure (MSLP) data were sourced from the fifth generation
163 of ECMWF's ERA5 reanalysis. This reanalysis provides a comprehensive record of global climate and weather from
164 the last 4 to 7 decades. ERA5 integrates observational data with atmospheric models to deliver detailed and accurate
165 assessments of past weather. It has a horizontal resolution of 0.25° for latitude and longitude, a temporal resolution of
166 one hour, and a vertical resolution based on 37 pressure levels (Hersbach et al., 2020a; 2020b). The study area spans
167 from 6°W to 42°E and 30°N to 48°N (Figure 1a, inset map), encompassing the region where key synoptic processes
168 influencing the Adriatic Sea predominantly occur. The analysis covers a 40-year period from 1979 to 2019, providing
169 a comprehensive temporal dataset for assessing atmospheric conditions. At the same time, this area optimizes the
170 calculation time.

171
172 To manage the large datasets of 10-meter wind and MSLP and classify them into spatio-temporal patterns that shed
173 light on atmospheric conditions favoring fog formation at Pula Airport, the Growing Neural Gas Network (GNG)

Commented [M2]: New paragraph started

174 method was employed. GNG is an unsupervised artificial neural network that clusters high-dimensional input data by
175 reducing its dimensions and grouping it into best matching units (BMUs) (Fritzke, 1995). Unlike traditional neural
176 networks with fixed structures, GNG dynamically expands by adding new neurons in response to input patterns. This
177 ability to grow and adapt allows GNG to effectively cluster data and detect patterns and anomalies. The GNG
178 algorithm has been successfully used to detect anomalies in Adriatic Sea data, combining various biological and
179 oceanographic inputs (Šantić et al., 2021; Džoić et al., 2022).

180
181 In this study, the methodology described in Matić et al. (2022) was applied to a high-dimensional, hourly, 40-year
182 dataset comprising wind components u and v , analyzed separately for each month of the year. Prior to implementing
183 the GNG algorithm, the wind data was arranged in such a way that two columns represented the spatial variations of
184 u and v , while rows corresponded to temporal instances. Wind data over land was excluded and assigned as NaN
185 values to reduce calculation time. This exclusion did not affect the results, as the study's primary focus was on the
186 synoptic-scale influences that generate specific wind patterns conducive to the formation of fog and mist. Over the
187 sea, the winds are very homogeneous and are often directly related to large-scale synoptic systems such as cyclones
188 or anticyclones, ~~whereas~~ Over land, the influence of topography and vegetation introduces noise, ~~masking these~~
189 ~~processes~~ making it more difficult to distinguish synoptic influences from local influences. The proximity of the
190 airfield to the sea and the flat, low-lying terrain in the direction of prevailing winds (Figure 1b) justified this
191 simplification of calculations. The GNG algorithm, implemented using the NeuPy Python library and parameterized
192 following Matić et al. (2022), was used to calculate 9 BMUs per month for each month of the year. These BMUs were
193 then linked to corresponding mean sea level pressure (MSLP) fields. The temporal sequence of BMUs was utilized to
194 compute an average pressure field for each BMU, offering a detailed representation of atmospheric patterns associated
195 with fog formation.

196
197 Data processing and visualization were conducted using Python and MATLAB, with MATLAB employing the
198 M_map mapping package (Pawlowicz, 2020), available at www.eoas.ubc.ca/~rich/map.html.

199

200

201

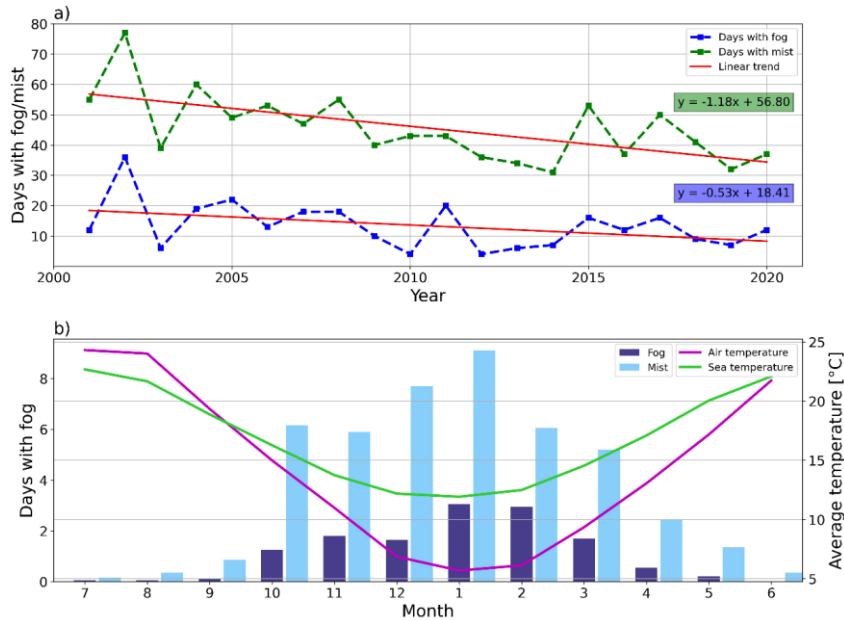
202

203

Commented [MZ3]: Rephrased the sentence to make it more clear

204 **3 Results and discussion**

205 **3.1 Climatological analysis**



206
207 **Figure 2. a) Annual number of days with fog (blue line) and mist (green line) at Pula Airport, 2001-2020. with associated**
208 **linear trends and trend equations. b) Average monthly number of days with fog and mist at Pula Airport, the average sea**
209 **temperature measured at the oceanographic station in Pula Bay and the average air temperature measured at the Pula**
210 **Airport, 2001-2020. The graph is centered on the boreal winter.**

Commented [MZ4]: Typo corrected

211 To comprehensively analyze fog occurrence over Pula Airport, a climatological analysis was conducted at both large
212 and small scales. Figure 2a illustrates the annual number of days with fog and mist from 2001 to 2020. A "fog day" is
213 defined as any day with at least one METAR report indicating visibility below 1 km and the presence of fog at the
214 airport. Similarly, a "mist day" is defined as any day with a METAR report indicating visibility between 1 km and 5
215 km, accompanied by mist observation, consistent with aeronautical meteorology definitions. This approach excludes
216 cases where reduced visibility was caused by precipitation, such as rain or drizzle. On average, Pula Airport
217 experiences 13.4 fog days and 45.6 mist days per year; however, this number is steadily decreasing, as indicated by
218 the pronounced negative trend. The Mann-Kendall statistical significance test shows that this result is statistically
219 significant at the 95% confidence level. A detailed evaluation of the linear trend indicates that the average number of
220 fog days decreased by more than 10 days, from 18.4 in 2001 to 8.3 in 2020, with a slope coefficient of -0.53. Similarly,
221 the average number of mist days declined by over 22 days, from 56.8 in 2001 to 34.4 in 2020, with a slope coefficient
222 of -1.18. The larger absolute value of the slope coefficient for mist suggests that the average number of mist days is
223 declining at a faster rate.

224

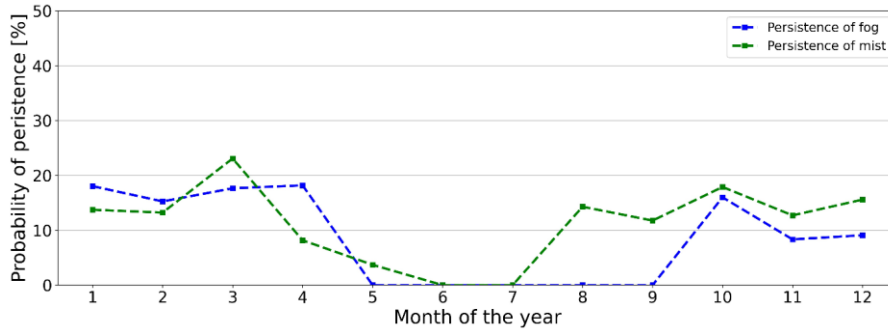
225 The observed statistically significant decreasing trend in the frequency of fog and mist at the airport is consistent with
226 similar findings in Europe, such as at Zagreb Airport (Zoldoš and Jurković, 2016) and Milano Airport (Mariani, 2009).
227 While the decrease in Zagreb and Milan is largely attributed to reduced air pollution, this conclusion is more
228 challenging to apply to Pula. As a smaller city with less industrial development, Pula's impact on neighboring
229 suburban and rural areas is not as pronounced. While a decrease in fog and mist frequency has been observed across
230 Europe, the effect is more prominent in continental Europe than in the Mediterranean region (Vautard et al., 2009).
231
232 Global warming and climate change are key drivers behind the long-term decline in fog frequency. Contributing
233 factors include rising temperatures in Pula and the surrounding Istria region (Bonacci, 2010; Šimunić et al., 2021).
234 increased sea surface temperatures (SST) throughout the Mediterranean (Pastor et al., 2018) and global trends in ocean
235 stratification (Li et al., 2020). Climate model reanalysis for the Adriatic Sea from 1987 to 2017 shows clearly positive
236 SST trends, especially in summer (Tojčić et al., 2023). Positive wind trends have been observed over the sea and along
237 the Adriatic Coast, between 0.1 and 0.2 m s⁻¹ per decade (Tojčić et al., 2023), which could influence fog formation.
238 Furthermore, future projections suggest these changes will intensify, including lower wind speeds in coastal areas and
239 more extreme contrasts such as increased droughts and heavy precipitation events (Tojčić et al., 2024). Warmer SSTs
240 influence fog formation in two ways. Generally, they increase evaporation rates, enhancing fog advection when winds
241 are favorable. Additionally, in cases where fog forms with SST < SAT, they reduce the temperature gradient required
242 for fog development.~~Warmer SSTs reduce the temperature gradient required for fog formation and increase~~
243 ~~evaporation rates, promoting fog advection when winds are favorable.~~ In Pula, these favorable winds, which blow
244 over the sea, play a significant role in fog and mist formation.

245
246 A seasonal analysis (Figure 2b) reveals that over 90% of fog and mist events occur between October and March.
247 January accounts for the highest frequency of fog (23% of days) and mist (20% of days), followed by February (21%
248 and 13%, respectively), with December notable for mist (17%). In March, October, and November, fog and mist occur
249 on 12–13% of days. Fog is rare from April to May and almost absent from June to September; for example, no fog
250 was observed in June during the analyzed period. The annual distribution of fog at Pula Airport is also comparable to
251 the annual distribution of fog events at Zagreb Airport (Zoldoš and Jurković, 2016). A summary of the data shows
252 that during the climatological summer (June-July-August), fog occurrence can be expected approximately every six
253 years. Mist follows a similar seasonal pattern but is more frequent overall. In recent decades, January and February
254 have swapped positions as the months with the highest frequency of fog. While February used to be the foggiest month
255 at Pula Airport with an average of 3.5 foggy days (Stipaničić, 1972), climatological results have shown us that January
256 has become the foggiest month with 3.05 foggy days. The frequency of fog persistence, which is defined as fog
257 occurrence on two consecutive days, is shown in Figure 3. As expected based on previous findings about fog
258 characteristics, persistence can be expected only in the colder part of the year (October-April). From May to
259 September, there have been no recorded instances of fog occurring on two consecutive days. Stable anticyclonic
260 conditions during the cold season are most conducive to fog persistence.

Commented [MZ5]: Text moved from the conclusion

Commented [MZ6]: Sentence rephrased

Commented [MZ7]: Text moved from the conclusion

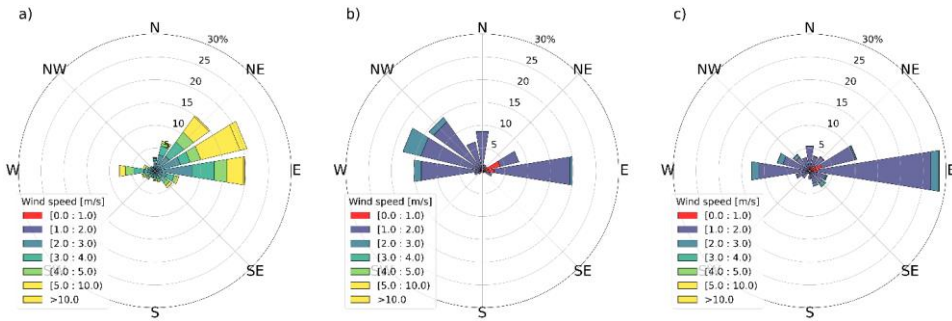


261
 262 **Figure 3. Yearly distribution of the climatological probability of persistence (fog occurrence on two consecutive days) of fog**
 263 **and mist at Pula Airport, 2001-2020. The probability of persistence is defined as the number of days with persistence relative**
 264 **to the total number of days with fog in a given month. Cases where a single fog event was present around midnight (and**
 265 **thus spanned two days) were not counted as persistence.**

266 Wind is a critical factor influencing the formation and persistence of fog, as turbulence from wind shear significantly
 267 impacts the height of the stable boundary layer. To understand this relationship, the statistical characteristics of wind
 268 during fog episodes were analyzed. Figure 4 shows wind distributions (data from METAR reports) for all conditions
 269 and for fog/mist conditions in a wind rose plot. In general, the dominant wind at Pula Airport is the NE (*bora*), which
 270 can easily reach speeds greater than 10 m s^{-1} . Other frequently observed winds include westerlies, resulting from the
 271 interaction of Etesian winds with the sea breeze circulation (Pandžić and Likso, 2005; Klaić et al., 2009), as well as
 272 north-northeasterly and southeasterly winds. Winds from the northwest and southwest are relatively rare. The wind
 273 rose for fog conditions (Figure 4b) contrasts sharply with general conditions; W/NW winds are the most common
 274 (accounting for 47.7% of measurements). These winds blow from the direction of the open sea, whereas easterly winds
 275 blow from Kvarner Bay, characterized by deeper waters and numerous islands. In some cases, fog also forms under
 276 light easterly winds, typically below 3 m s^{-1} , although westerly fog events are often accompanied by wind speeds
 277 exceeding this threshold. Southerly winds are rarely associated with fog at Pula Airport.

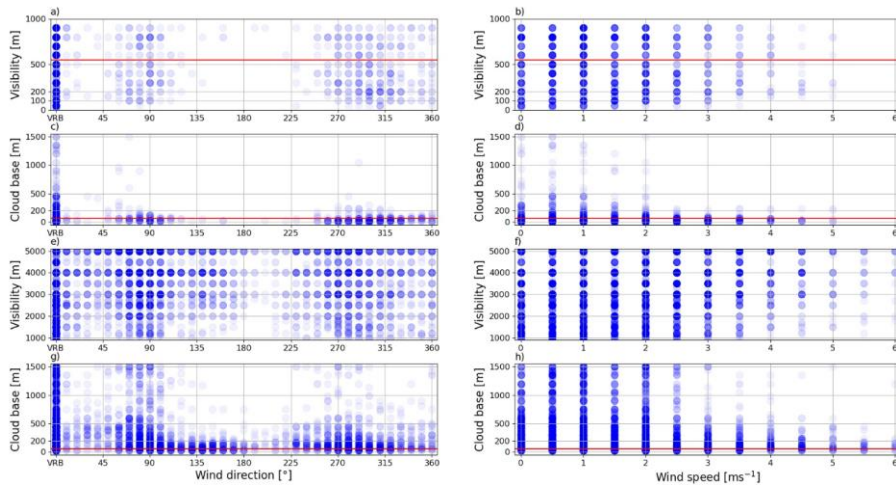
278
 279 Mist conditions show a different wind pattern (Figure 4c). Unlike fog, mist frequently occurs with easterly winds,
 280 which account for 28.8% of observations. This is consistent with the higher overall occurrence of mist compared to
 281 fog (Figure 2). Further analysis of the relationship between wind and visibility/cloud base in fog conditions (Figure
 282 5a-d) highlights the rarity of fog in situations with northerly winds. The scatter plot of visibility and wind speed
 283 confirms the existence of an optimal range of wind speeds conducive to fog, with most fog events occurring at wind
 284 speeds between 0 and 2 m s^{-1} . The same is also observed for low clouds (lower than 200 m) — the majority of low
 285 cloud bases were observed at wind speeds of 1 m s^{-1} or less, some between 1 and 2 m s^{-1} , and very few cases at higher
 286 wind speeds. The absence of cloud bases above 300 m at wind speeds higher than 2 m s^{-1} is interesting. Higher wind
 287 speeds indicate stronger advection, and personal communication from forecasters suggests that in these cases cloud
 288 bases can be very low. This is particularly evident under westerly flows, where fog is more common and where wind
 289 speeds are higher. The data for mist conditions (Figure 5e-h) leads to similar conclusions for visibility—mist occurs

290 more frequently under westerly or easterly winds with slightly higher wind speeds than fog. Mist conditions with
 291 cloud bases above 500 m do occur but are rare, and one noteworthy difference between mist and fog is the higher
 292 number of mist events with a low cloud base during southeasterly and southwesterly winds.
 293



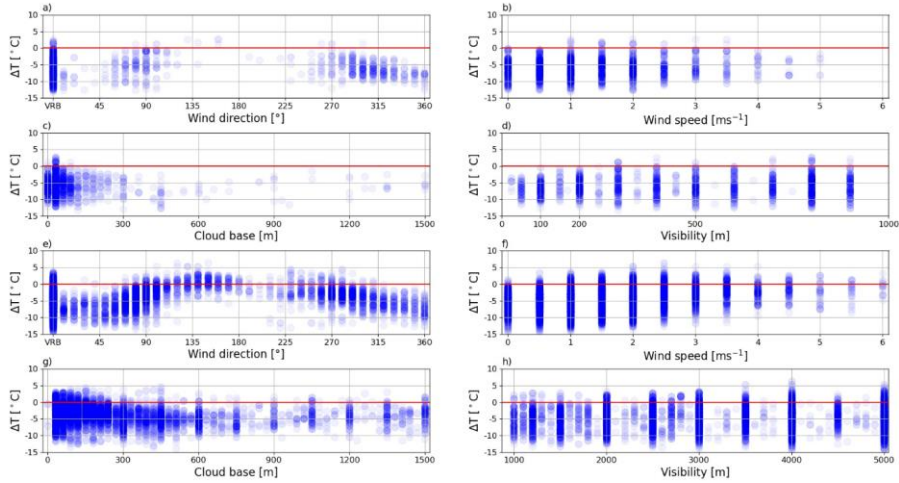
294
 295 **Figure 4.** Wind rose plots for Pula Airport, for dataset in the period 2001-2020: (a) the whole dataset, (b) fog conditions (c)
 296 mist conditions. Data includes only reports where the variation in direction is less than 60° according to ICAO definition.
 297 These account for 74 % of total data, 36 % of data in fog conditions and 39% of data in mist conditions.

Commented [MZ8]: Improved figure – wind speeds <1m/s marked in red;



298
 299 **Figure 5.** Scatter plots of various meteorological parameters for fog conditions (a-d) and mist conditions (e-h) at Pula
 300 Airport, 2001-2020. Circles are colored according to the frequency of data points (darker – more frequent). Red lines mark
 301 the limits for Category I takeoff-landing procedures mentioned in Chapter 2. “VRB” denotes variable wind direction (180°
 302 or more in a 2-minute interval) according to definition by ICAO (International Civil Aviation Organization).

303
 304



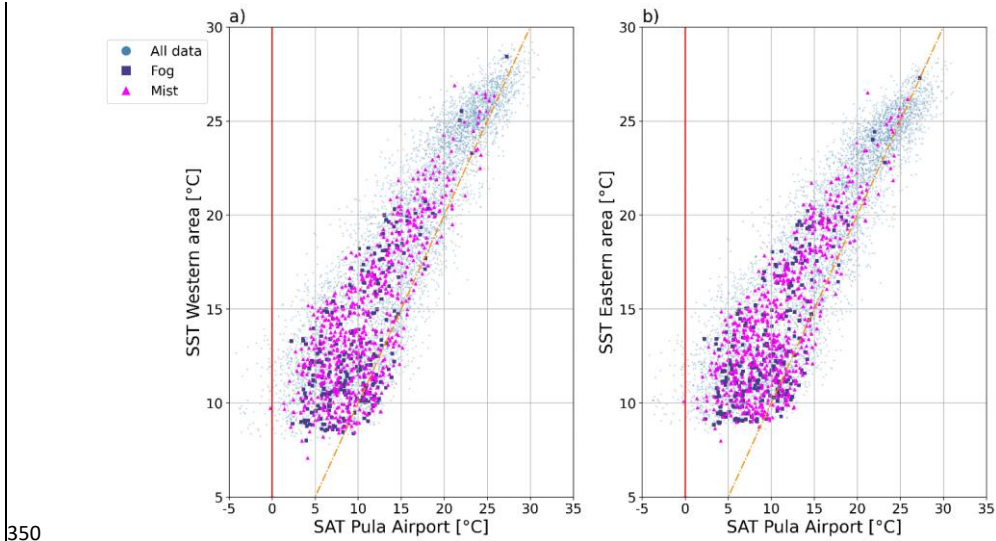
305
 306 **Figure 6.** Scatter plots of air-sea temperature difference between Pula Airport and Pula oceanographic station and various
 307 meteorological parameters at fog initiation (a-d) and mist initiation (e-h), 2001-2020. Circles are colored according to the
 308 frequency of data points (darker – more frequent). Red lines mark the 0 °C difference between air and sea temperature.
 309 “VRB” denotes variable wind direction (180° or more in a 2-minute interval) according to definition by ICAO
 310 (International Civil Aviation Organization).

311
 312 Fog occurrence can also be analyzed by examining conditions leading up to or at the time of its formation, as
 313 demonstrated in previous studies (Tardif and Rasmussen, 2007; Veljović et al., 2015; Zoldoš and Jurković, 2016), or
 314 by investigating the difference between air and sea surface temperature for marine fog (Li et al., 2022). In this study,
 315 SAT data from METAR reports at Pula Airport were compared with SST measurements from the oceanographic
 316 station in Pula Bay. Figures 6a-d depict scatterplots of SAT-SST differences and various parameters at fog initiation
 317 (first METAR report with visibility <1000 m), while Figures 6e-h present similar data for mist initiation.

318
 319 The majority of fog and mist events occur under negative SAT-SST differences, indicating that the sea surface is
 320 warmer than the overlying air. Fog rarely forms during southerly winds, but mist is more common in these conditions,
 321 particularly under southeasterly winds (Figure 6e). For southeasterly, southerly, and southwesterly winds with mist,
 322 the SAT-SST difference tends to approach 0. Among fog events, 97.4% occurred with negative SAT-SST differences,
 323 with only 2.6% forming under conditions where SAT is equal to or warmer than SST. In mist cases, the proportion of
 324 positive or zero SAT-SST differences is slightly higher (7.4%) but still strongly favors conditions with warm sea and
 325 cooler air. At Pula Airport, fog is more common at wind speeds above 3 m s⁻¹ than in continental areas such as Zagreb
 326 Airport (Zoldoš and Jurković, 2016), but less common than in coastal regions such as California, where fog occurs at
 327 speeds above 10 m s⁻¹ (Filonczuk et al., 1995). Fog rarely occurs in calm conditions (Figure 4b), suggesting an optimal
 328 wind speed range for its formation and warranting further exploration, as the role of wind speed on turbulence and
 329 surface heat fluxes, as highlighted by Gultepe et al. (2007), significantly influences fog. While the influence of SST
 330 was initially assessed by comparing SAT measurements from the airport with SST data from the oceanographic

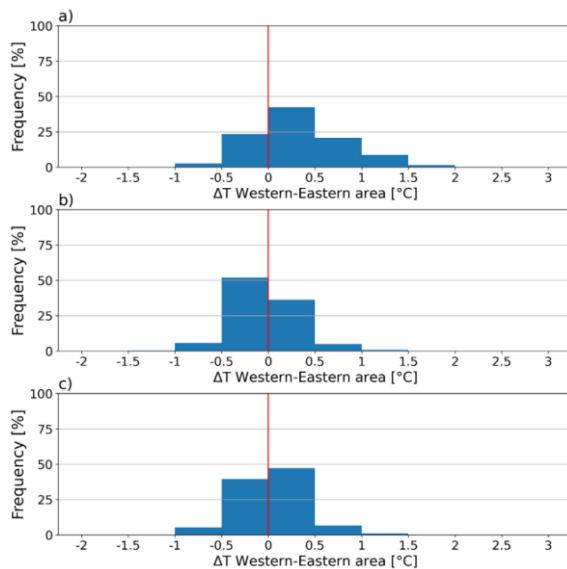
331 station, a more comprehensive understanding is obtained by examining the effect of the sea to the west and east of the
 332 airport. To achieve this, satellite-derived SST values for the regions west and east of the airport (Figure 1b) were
 333 analyzed. These areas correspond to the directions of the two prevailing winds most commonly associated with fog
 334 formation at Pula Airport. Scatterplots of SAT versus SST were generated for the eastern and western regions,
 335 encompassing all observations, as well as those specifically under fog and mist conditions (Figure 7). A visual analysis
 336 indicates that fog and mist typically form when SAT-SST pairs are associated with lower values. A more detailed
 337 analysis reveals that fog data points (squares) in the western region are more dispersed, indicating greater
 338 variability in SST for the same SAT, while the eastern region shows a more consistent SST-SAT relationship.
 339 Statistical analysis supports this observation, with the standard deviation of SST for fog observations being 3.55 °C
 340 in the western area and 3.37 °C in the eastern area. For mist, the standard deviation is 4.03 °C in the western area and
 341 3.83 °C in the eastern area. To further investigate the role of SST in fog formation, differences in
 342 SST between the western and eastern regions were analyzed under various conditions (Figure 8). When neither fog
 343 nor mist is present, SST in the western area is slightly higher than in the eastern area. During fog events, however, the
 344 pattern reverses, with SST being higher in the eastern area. In contrast, mist typically occurs when SST is higher in
 345 the western area than in the eastern area. These differences align with the prevailing wind directions observed during
 346 fog and mist events (Figure 4). During fog, winds that are predominantly from the west to northwest (W-NW) promote
 347 cooling in the western area. Winds from the east (E) during mist contribute to reduced SST in the eastern region.
 348 Despite these variations, the SST differences between the two areas are small, rarely exceeding 0.5 °C.
 349

Commented [MZ9]: Figure altered for clarity reasons



350
 351 **Figure 7. Scatter plots of satellite sea surface temperature (SST) for western area (a) and eastern area (b), and surface air**
 352 **temperature (SAT) at Pula Airport, 2001.-2020. The vertical red line indicates SAT=0 °C, and the dotted diagonal orange**
 353 **line indicates SAT=SST.**

Commented [MZ10]: Improved captions



354

355 **Figure 8. Histograms of satellite SST difference between the western and eastern area for observations without fog and**
 356 **mist (a), fog (b) and mist(c).**

Commented [MZ11]: Corrected phrase

357 **3.2 GNG analysis of synoptic weather patterns**

358 In this analysis, the GNG method was applied to identify characteristic temporal and spatial patterns in wind and
 359 MSLP fields associated with the formation of fog and mist in the Pula region. The analysis was conducted on a monthly
 360 basis, processing data for each month (e.g., all January data, all February data) separately. This approach was chosen
 361 to improve the interpretability of the results, to take seasonality into account and to reduce the computational effort,
 362 especially given the large size of the hourly dataset. To save resources, the GNG algorithm was applied exclusively
 363 to 10 m wind data from ERA5, with the derived pressure fields being extrapolated afterwards. The derived pressure
 364 field corresponds to the mean pressure field associated with each BMU. Once the BMUs were identified, all pressure
 365 fields corresponding to the time instances of each BMU were retrieved and averaged to calculate the mean pressure
 366 field for each BMU. To obtain an appropriate synoptic situation with large wind systems, such as anticyclones and
 367 cyclones affecting the northern Adriatic, a large area in the Mediterranean was selected for analysis (Figure 1b). The
 368 analysis utilized 40 years of ERA5 data (1979–2019), providing extensive time series data to enable the GNG
 369 algorithm to derive robust and accurate spatio-temporal patterns. Notably, there is a one-year discrepancy between the
 370 ERA5 dataset and the fog dataset (2020) due to the GNG analysis being completed before this study began, and the
 371 computational resources required for a new analysis were unavailable. Since the wind was the primary variable and
 372 the MSLP was derived by averaging numerous synoptic situations, the wind had the dominant influence. This
 373 approach excluded the occurrence of extreme cyclonic systems (MSLP < 1000 hPa) or anticyclonic (MSLP > 1030
 374 hPa) from the results. For example, deep cyclones, which are extremes, are smoothed, and while BMUs can indicate

375 their locations, the exact pressure values are not retained. However, from a conceptual point of view, the interaction
 376 between high and low pressure systems and the location of these systems and their associated winds match well with
 377 the climatology of the region.

378
 379 This process generated 9 Best Matching Units (BMUs) for each month (a total of 108 BMUs) distributed across hourly
 380 data, representing the weather patterns with the highest variance. Hourly data were then aggregated into daily data by
 381 identifying the most frequently occurring BMU within a day. For the 2001–2019 period, each day with fog or mist was
 382 assigned to its corresponding dominant BMU, providing a synoptic weather pattern classification for fog and mist
 383 days at Pula Airport. To focus on the prevailing synoptic patterns that contribute to the formation of fog and mist, the
 384 months from October to March (Figure 2b) were examined in more detail (Table 1). In this way, 85 % of the variability
 385 could be captured. Then, for each month, the first BMUs whose sum of their contributions to the variability exceeded
 386 the threshold of 60 % were selected. In this way, a total of 18 BMUs were included in the further analysis, which is
 387 significantly fewer than 54 BMUs (6 months multiplied by 9 BMUs). By selecting 2 to 4 BMUs for each month based
 388 on the criteria described above, the study captured more than 60 percent of the events for each analyzed month.

389
 390
 391
 392
 393

394 **Table 1. Display of the most frequent Best Matching Units (BMUs) (the first BMUs for each month whose sum of their**
 395 **contributions to the variability exceeded the threshold of 60 %) describing the prevailing synoptic weather pattern during**
 396 **the days with fog and mist for the selected month at Pula Airport, 2001-2019. The slope coefficients describe the linear**
 397 **trends of the most common BMUs, i.e. the yearly change in frequency, and they are also used to generate the graphs of the**
 398 **linear trends in Figure 14.**

Month	BMU	Synoptic pattern	Wind	Slope coeff.	Frequency (fog)		Frequency (mist)	
					#	%	#	%
January	BMU-1-6	Quasi-non-gradient-field	WNW, W	-0.390	30	54 %	68	39 %
	BMU-1-8	Cyclone over northern Adriatic (MSLP<1008 hPa)	NW	0.107	11	20 %	39	23 %
February	BMU-2-5	Anticyclone over central/western Europe (MSLP>1028 hPa)	NE, NNE	0.006	8	16 %	13	12 %
	BMU-2-6	Quasi-non-gradient-field	SSW	-0.138	17	33 %	36	32 %
	BMU-2-7	Cyclone over northern Adriatic (MSLP<1008 hPa)	NW	-0.025	7	14 %	59	38 %
March	BMU-3-1	Anticyclone over southeastern Europe (MSLP>1022 hPa)	SSE	-0.572	16	16 %	5	16 %
	BMU-3-3	Cyclone over northern Adriatic (MSLP<1006 hPa)	SE	-0.051	6	19 %	25	25 %
	BMU-3-8	Quasi-non-gradient-field	SSE	0.255	11	35 %	31	39 %
October	BMU-10-1	Anticyclone over southeastern Europe (MSLP>1018 hPa)	NE	0.158	4	16 %	13	11 %
	BMU-10-5	Anticyclone over southeastern Europe (MSLP>1020 hPa)	SE	-0.272	10	40 %	38	32 %

	BMU-10-6	Quasi-non-gradient-field	SE	-0.051	4	16 %	27	23 %
November	BMU-11-5	Anticyclone over eastern Europe (MSLP>1024 hPa)	SE	0.251	8	24 %	23	21 %
	BMU-11-7	Quasi-non-gradient-field (MSLP>1022 hPa)	WSW	-0.415	6	18 %	29	26 %
	BMU-11-9	Anticyclone over southeastern Europe (MSLP>1026hPa)	ENE	-0.041	11	33 %	28	25 %
December	BMU-12-1	Anticyclone over southeastern Europe (MSLP>1026 hPa)	S	-0.000	7	21 %	31	21 %
	BMU-12-3	Cyclone over southern Adriatic (MSLP<1008 hPa)	NE	0.266	5	15 %	23	15 %
	BMU-12-4	Cyclone over the Tyrrhenian Sea (MSLP<1008 hPa)	NE	-0.470	6	18 %	14	9 %
	BMU-12-8	Anticyclone over central and eastern Europe (MSLP >1030 hPa)	NE	-0.130	3	9 %	23	15 %

399

400 The analysis of synoptic patterns associated with fog formation (Table 1) indicates that in January, the dominant
401 conditions favoring fog and mist in Pula are characterized by a quasi-non-gradient field across the region (BMU-1-6,
402 Figure 9a), with a very weak mean pressure gradient (Belušić Vozila et al., 2021). This stable atmospheric pattern
403 supports the persistence of calm and stagnant air masses over Pula, limiting the dispersion of moisture and pollutants
404 and thereby enabling fog formation. The second most common synoptic pattern conducive to the formation of fog and
405 mist features a cyclone over the northern Adriatic (BMU-1-8, Figure 9c). Both synoptic patterns support weak
406 WNW/NW winds over the Istrian peninsula (Figure 9b and 9d). A similar synoptic pattern persists during the transition
407 into February and March. The cyclone over the northern Adriatic is the most frequent pattern suitable for the formation
408 of mist in February (BMU-2-7, Figure 10a) and the second most frequent in March (BMU-3-3, Figure 10e). The
409 difference is the prevailing NW wind in February (Figure 10b), while March is characterized by SE winds (Figure
410 10f). The quasi-non-gradient pressure field is the most common pattern favorable for both fog and mist formation in
411 March (BMU-3-8, Figure 10g), and the second most common for fog and the most common for mist in February
412 (BMU-2-6, Figure 9g). SSW winds are observed in February (Figure 9h), whereas March is associated with weaker
413 SSE winds (Figure 10d). In addition to the quasi-non-gradient field, favorable synoptic patterns in both February and
414 March also include anticyclones over continental Europe (BMU-2-5, Figure 9e and BMU-3-1, Figure 10c).

415

416 Fog events are rare in Pula from April to September, and as a result, the BMU analysis does not reveal clear patterns.
417 The infrequent occurrence of fog during this period is attributed to lower relative humidity and the more stable
418 atmospheric conditions typical of summer in the region. However, local factors, such as the sea/land breeze, may
419 influence fog formation. Therefore, any analysis based on data from these months should be interpreted with caution,
420 as the number of recorded fog events is limited.

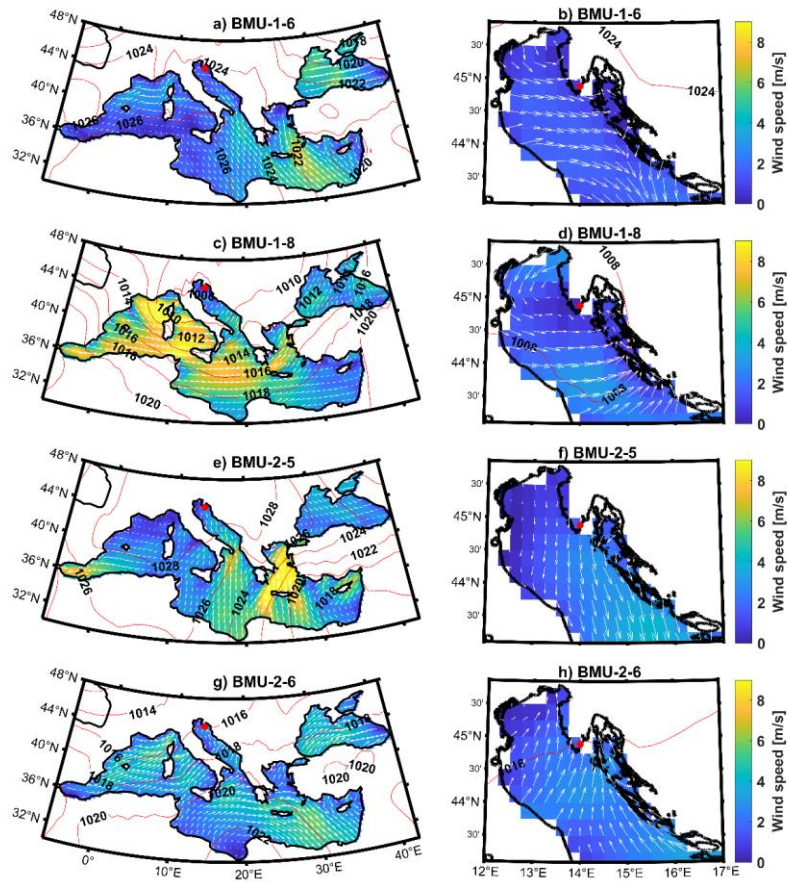
421

422 At the beginning of October, synoptic conditions favorable for the occurrence of fog and mist in Pula are typically
423 characterized by high pressure over continental Europe, with the most common pattern being the center of the high-
424 pressure system positioned over southeastern Europe, which supports SE winds (BMU-10-5, Figure 11c and 11d).

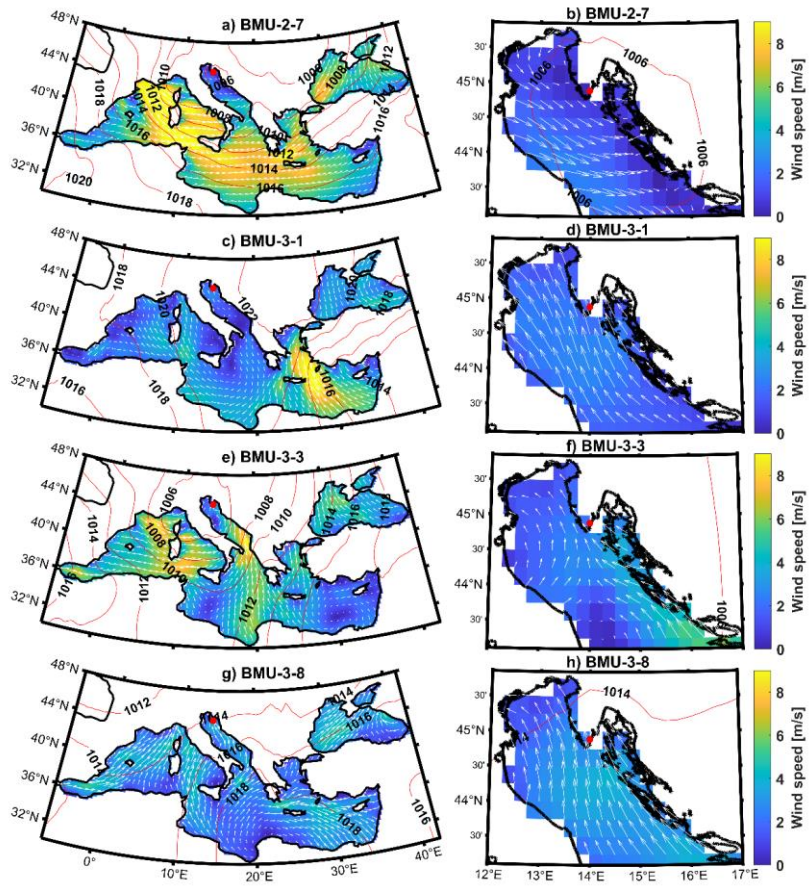
425 This anticyclonic pattern persists into November, accompanied by a strengthened pressure field and intensified
426 pressure gradients over the central Mediterranean, conditions which promote fog development in the region (BMU-
427 11-9, Figure 12e and 12f). The intensified synoptic pressure gradients over the central Mediterranean contribute to
428 increased NE wind patterns. This increased wind activity can result in moist air being transported from the sea to the
429 coastal regions, providing an additional source of moisture for fog formation. The convergence of air masses along
430 these enhanced pressure gradients likely induces upward motion of air, which can result in adiabatic cooling and an
431 increase in relative humidity, creating conditions favorable to fog and mist formation. Pula's coastal location amplifies
432 the influence of the anticyclone. Coastal areas are more prone to temperature inversions due to the sea's heat retention,
433 which reduces temperature fluctuations. Anticyclonic conditions over Eastern Europe combined with coastal
434 geography create an environment where cool, moist air is trapped near the surface, favoring the formation of fog. The
435 conditions that favor mist formation are varied; the most common synoptic pattern is the one where the high-pressure
436 area is located over the western Mediterranean and WSW winds over the Istrian peninsula. In addition to the
437 anticyclone, a quasi-non-gradient field is also present in October and November (BMU-10-6, Figure 11e, 11f and
438 BMU-11-7, Figure 12c and 12d). In December, the prevailing synoptic weather patterns associated with fog and mist
439 become harder to identify, with BMUs more evenly distributed and more dynamic conditions, similar to those in
440 February and March. Nonetheless, the most frequent synoptic pattern for fog and mist (BMU-12-1, Figure 13a and
441 BMU-12-8, Figure 13g) has anticyclonic characteristics. Under these conditions, the Pula region is under the influence
442 of a pressure ridge, with the prevailing weak wind patterns from the S and NE further increasing the probability of
443 fog formation (Figure 13b and 13h). Compared to earlier months, cyclones also play a more pronounced role in
444 December's fog and mist formation. This influence is observed in two ways: weak NE winds associated with cyclonic
445 conditions in the southern Adriatic (BMU-12-3, Figure 13c, 13d) and stronger NE winds due to cyclonic conditions
446 in the Tyrrhenian Sea (BMU-12-4, Figure 13e, 13f).

447
448 In summary, most fog and mist events during the cold season occur under stable anticyclonic or quasi-non-gradient
449 conditions (13 total), though some events also occur under low-pressure conditions (5 total). WNW/W winds are most
450 common in January and February under quasi-non-gradient fields and they contribute significantly to fog formation.
451 SE winds dominate in March and October under anticyclonic conditions. Northeasterly winds are predominant in
452 December, often in conjunction with anticyclones. The quasi-non-gradient field is the most-frequent weather situation,
453 accounting for 40% of fog cases and 37% of mist cases, followed by anticyclones, which account for 39% of fog cases
454 and 33% of mist cases. Cyclones are less common, accounting for 21% of fog cases and 30% of mist cases.

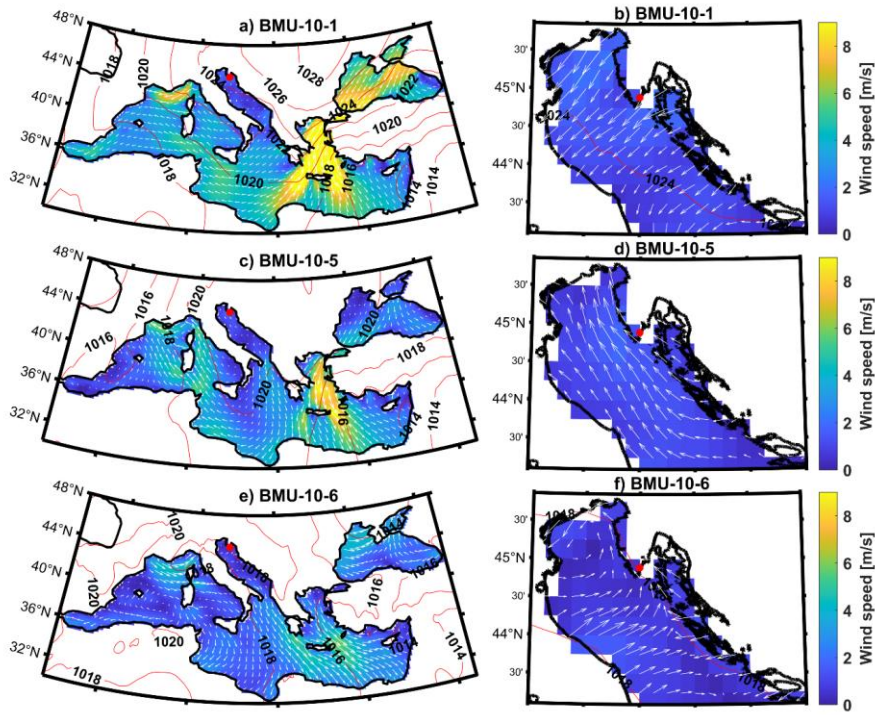
Commented [MZ12]: corrected



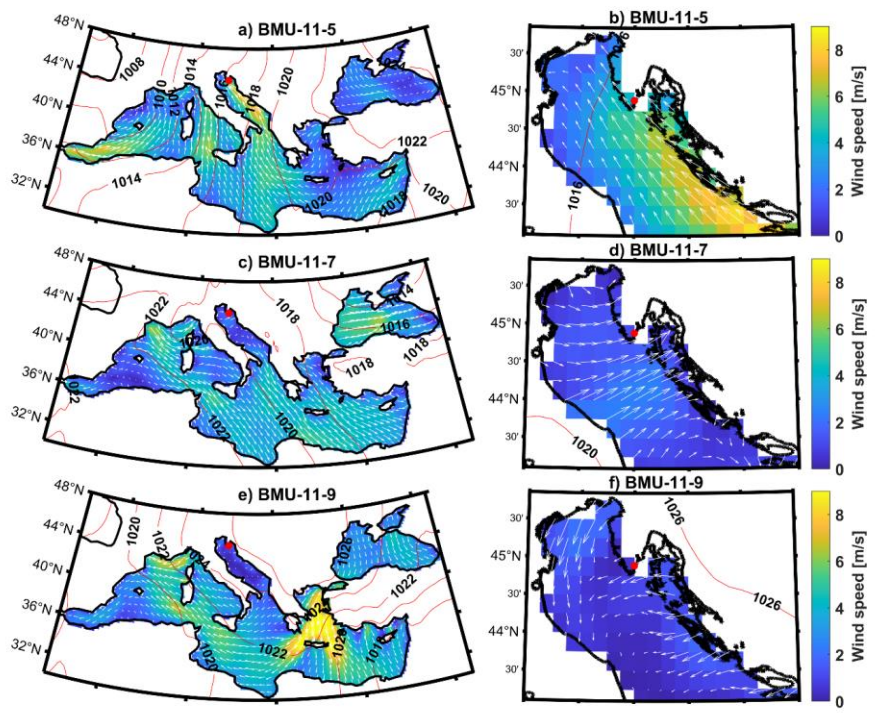
455
 456 Figure 9. Prevailing Best Matching Units (BMUs) describing the synoptic patterns favoring the formation of fog and mist
 457 at Pula Airport in January (a, c) and February (e, g) for the wider Mediterranean region. The red dot marks the location
 458 of Pula Airport. The red contour lines show the mean sea level pressure (MSLP). The contours represent the amplitude of
 459 the wind speed, above which the wind vectors are represented by arrows (every third vector has been drawn). The same
 460 principle applies to the zoomed area of the northern and central Adriatic for January (b, d) and February (f, h), but here
 461 each vector is plotted.
 462



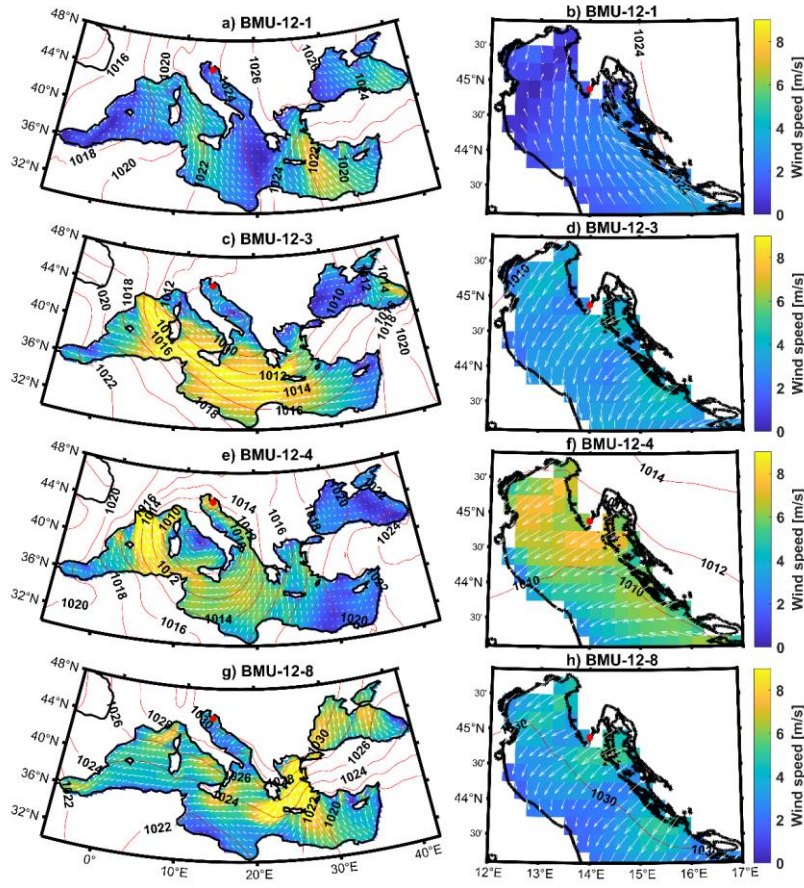
463
 464 Figure 10. Similar to Figure 9, but for February (a) and March (c, e, g) in the wider Mediterranean area, and for the
 465 northern and central Adriatic: February (b) and March (d, f, h) in the zoomed-in area.



467
 468 Figure 11. Similar to Figure 9, but for October: (a, c, e) show the wider Mediterranean area, while (b, d, f) focus on the
 469 northern and central Adriatic.



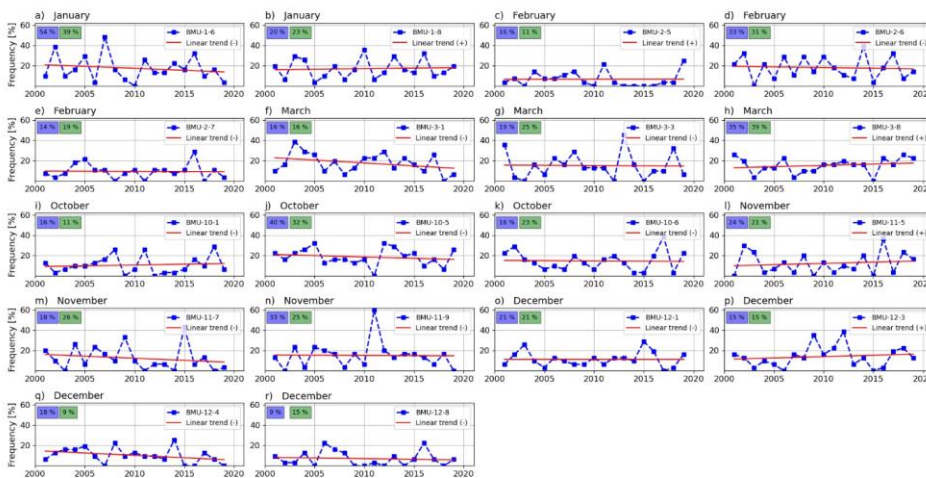
470
 471 Figure 12. Similar to Figure 9, but for November: (a, c, e) show the wider Mediterranean area, while (b, d, f) focus on the
 472 northern and central Adriatic.



473
 474 Figure 13. Similar to Figure 9 but for December: (a, c, e, g) show the wider Mediterranean, while (b, d, f, g) focus on the
 475 northern and central Adriatic.
 476
 477
 478
 479
 480
 481
 482
 483
 484
 485
 486
 487
 488

489 In addition to examining the prevailing synoptic patterns during the occurrence of fog and mist, the GNG analysis
 490 also allows for the investigation of the time series of frequencies of individual BMUs. This was accomplished by first
 491 calculating the relative monthly frequency of each BMU for each year, followed by using linear regression to estimate
 492 trends and calculate slope coefficients. This process provides insights into changes in the frequency of each BMU
 493 over two decades (Table 1, Figure 14). In January, the more frequent BMU-1-6 (Figure 14a) has a strong negative
 494 trend of -0.390, while the less frequent BMU-1-8 (Figure 14b) has a weaker positive trend of 0.107. In February, the
 495 most frequent BMU-2-7 (Figure 14e) has a weak negative trend of -0.025. In March, the most frequent BMU, BMU-
 496 3-8 (Figure 14h) has a positive trend of 0.255, while BMU-3-1 (Figure 14f) has a strong negative trend of -0.572. In
 497 October, the most frequent BMU for fog and mist (BMU-10-5, Figure 14j) has a negative trend (-0.272), while in
 498 November and December there is almost no trend for the most frequent BMUs (BMU-11-9, Figure 14n and BMU-
 499 12-1, Figure 14o). It can be summarized from the table that the BMUs most associated with the occurrence of fog and
 500 mist exhibit negative trends in the months with the highest share, January and February. Analyzing the data by
 501 counting positive and negative changes and grouping the synoptic patterns into three categories
 502 (cyclonic/anticyclonic/quasi-non-gradient field) reveals that out of the 18 BMUs, 8 are anticyclonic, 5 are quasi-non-
 503 gradient, and 5 are cyclonic. There is no trend for BMU-12-1 in the anticyclonic group; 3 BMUs increase in frequency
 504 and 4 BMUs decrease in frequency. In the quasi-non-gradient group, there is 1 increase and 4 decreases. This decline
 505 in quasi-non-gradient synoptic situations has already been documented during the summer months (Belušić Vozila et
 506 al., 2021). Of the 5 cyclonic BMUs, 2 increase in frequency and 3 decrease. Additionally, a significant decrease (slope
 507 coefficient >0.3 or <-0.3) is observed in BMU-3-1 (anticyclonic), BMU-1-6 (quasi-non-gradient field), and BMU-12-
 508 4 (cyclonic). Positive trends do not show such large slope coefficients.

Commented [MZ13]: sentence from the conclusion moved here



509
 510 **Figure 14.** Relative frequencies and trends of most common (monthly share in days with fog/mist greater than 15%) BMUs
 511 for fog and mist in Pula Airport, data period: 2001-2019. Numbers shaded in blue denote the share of a BMU for fog days,
 512 numbers shaded in green denote the share of a BMU for mist days. The slope coefficient values for the linear trends can be
 513 found in Table 1.
 514

515 **4 Conclusion**

516 This comprehensive climatological analysis of fog and mist occurrences at Pula Airport from 2001 to 2020 has
517 provided valuable insights into the changing patterns of these meteorological phenomena. By combining classical
518 statistics and neural networks, the study produced noteworthy results.

519
520 ~~The observed statistically significant decreasing trend in the frequency of fog and mist at the airport is consistent with
521 similar findings in Europe, such as at Zagreb Airport (Zeldoš and Jurković, 2016) and Milano Airport (Mariani, 2009).
522 While the decrease in Zagreb and Milan is largely attributed to reduced air pollution, this conclusion is more
523 challenging to apply to Pula. As a smaller city with less industrial development, Pula's impact on neighboring
524 suburban and rural areas is not as pronounced. While a decrease in fog and mist frequency has been observed across
525 Europe, the effect is more prominent in continental Europe than in the Mediterranean region (Vautard et al., 2009).~~

526
527 ~~Global warming and climate change are key drivers behind the long-term decline in fog frequency. Contributing
528 factors include rising temperatures in Pula and the surrounding Istria region (Bonacci, 2010; Šimunić et al., 2021),
529 increased sea surface temperatures (SST) throughout the Mediterranean (Pastor et al., 2018) and global trends in ocean
530 stratification (Li et al., 2020). Climate model reanalysis for the Adriatic Sea from 1987 to 2017 shows clearly positive
531 SST trends, especially in summer (Tojčić et al., 2022). Positive wind trends have been observed over the sea and along
532 the Adriatic Coast, between 0.1 and 0.2 m s⁻¹ per decade (Tojčić et al., 2022), which could influence fog formation.
533 Warmer SSTs reduce the temperature gradient required for fog formation and increase evaporation rates, promoting
534 fog advection when winds are favorable. In Pula, these favorable winds, which blow over the sea, play a significant
535 role in fog and mist formation.~~

536 The frequency of occurrence of fog and mist at Pula airport has been decreasing, similar to trends observed in other
537 European locations. While reduced air pollution explains the decline in cities like Zagreb and Milan, this is less
538 applicable to Pula due to its smaller size and lower industrial impact. Climate change, including both rising air
539 temperatures as well as increased sea surface temperatures, is a key driver of this trend. Additionally, changing wind
540 patterns also influence fog formation by affecting temperature gradients and evaporation rates.

541
542 Fog at Pula airport occurs mainly during the cold season (October-March) and is primarily associated with weak
543 westerly and northwesterly winds. It is more likely to occur when the sea surface temperature is higher than the air
544 temperature. Mist has similar characteristics to fog, although it is more likely to occur with easterly winds. Wind
545 direction and SST variations between the sea to the west and east of the airport influence fog and mist formation.

546
547 Most fog and mist events during the cold season occur under stable anticyclonic or quasi-non-gradient conditions,
548 with the latter being the most frequent. Wind patterns vary seasonally, with WNW/W winds in January and February
549 aiding fog formation, SE winds prevailing in March and October, and northeasterly winds dominating in December
550 under anticyclones.

551

Commented [MZ14]: new, shorter text summarizing key points

Commented [MZ15]: summarizing findings from figures 4-13

552 ~~Analyzing the classified synoptic patterns — a key focus of this study — reveals that the patterns conducive to fog and~~
553 ~~mist generally have a negative trend. For example, quasi-non-gradient synoptic situations, the most common favorable~~
554 ~~pattern, have shown predominantly negative trends. This decline in quasi-non-gradient synoptic situations has already~~
555 ~~been documented during the summer months (Belušić Vozila et al., 2021). As these favorable synoptic patterns~~
556 ~~decrease, the accompanying winds that facilitate the advection of evaporated moisture from the sea to the land —~~
557 ~~strongly influenced by SST and air temperatures — are also reduced. Consequently, the number of days with fog and~~
558 ~~mist is expected to decline over time.~~

559 ~~Synoptic patterns that promote fog and mist, especially quasi-non-gradient situations, are declining. This reduction~~
560 ~~weakens winds that transport moisture from the sea to the land, influenced by rising sea surface and air temperatures.~~
561 ~~As a result, fog and mist frequency is expected to continue decreasing.~~

562
563 Overall, these findings provide a strong foundation for further research, facilitating a deeper understanding of the
564 meteorological and oceanographic factors that influence fog and mist at Pula Airport. This is especially significant as
565 it marks the first scientific study on fog in the Pula region in over 50 years, a period during which climate change has
566 notably impacted the local climate. ~~Future projections suggest these changes will intensify, including lower wind~~
567 ~~speeds in coastal areas and more extreme contrasts such as increased droughts and heavy precipitation events (Tojčić~~
568 ~~et al., 2024).~~ This study has taken on the broad task of identifying synoptic patterns conducive to fog and mist
569 formation. Since fog and mist are mainly influenced by wind speed and moisture advection, there is potential for
570 coupled atmospheric-oceanographic modeling that incorporates local topography and enhances the parameterization
571 of processes at finer temporal and spatial scales. Such advancements would provide a more comprehensive
572 understanding of local meteorological phenomena and their implications for various applications, including aviation
573 meteorology and environmental monitoring.

574 **Code/data availability**

575 All data and codes used in the analysis are available from the corresponding author on request.

576 **Author contribution**

577 Marko Zoldoš and Tomislav Džoić equally contributed to the conception and design of the study, material collection,
578 data preparation, statistical and neural network analysis, creation of the figures and writing. Frano Matic contributed
579 to the neural network analysis. All authors have read and approved the final manuscript.

580 **Competing interests**

581 The authors declare that they have no conflict of interest.

582 **Acknowledgments**

Commented [MZ16]: deleted because most of the content has been summarized in the main text (Figure 14)

Commented [MZ17]: new, shorter text summarizing key points

Commented [MZ18]: sentence moved to the main text

583 Frano Matić was supported in part by the European University of the Seas (SEA-EU) alliance through collaborative
584 efforts and resources. Measurements and observations for Pula Airport were provided by the Croatian Air Navigation
585 Service (Crocontrol Ltd.). SST data for Pula were provided by the Meteorological and Hydrological Service of Croatia
586 (DHMZ). SST data in the Mediterranean region were downloaded from the Copernicus Marine Data Store
587 (<https://data.marine.copernicus.eu/>). 10-m wind and mean sea-level pressure (MSLP) data were adopted from the fifth
588 generation of ECMWF's ERA5 reanalysis of global climate and weather. Final proofreading (grammar/spelling check)
589 was performed by ChatGPT from OpenAI.

590 **References**

- 591 Allan, S.S., Gaddy, S.G., Evans, J.E.: Delay causality and reduction at the New York City airports using terminal
592 weather information systems, Massachusetts Institute of Technology, Lincoln Laboratory, Project Rep. ATC-291,
593 2001
- 594 Belo-Pereira, M., Santos, J.A.: A persistent wintertime fog episode at Lisbon airport (Portugal): performance of
595 ECMWF and AROME models, *Meteorol. Appl.* 23, 353-370, doi:10.1002/met.1560, 2016
- 596 Bendix, J.: Fog climatology of the Po Valley, *Riv. Meteorol. Aeronau.* 54(3-4), 25-36, 1994
- 597 Belušić, A., Prtenjak, M.T., Güttler, I., Ban, N., Leutwyler, D., Schär, C.: Near-surface wind variability over the
598 broader Adriatic region: insights from an ensemble of regional climate models, *Clim. Dyn.* 50, 4455-4480,
599 doi:10.1007/s00382-017-3885-5, 2018
- 600 Belušić Vozila, A., Telišman Prtenjak, M., Güttler, I.: A weather-type classification and its application to near-surface
601 wind climate change projections over the Adriatic region, *Atmosphere* 12, 948, doi:10.3390/atmos12080948, 2021
- 602 Bergot, T., Koračin, D.: Observation, simulation and predictability of fog: review and perspectives, *Atmosphere* 12(2),
603 235, doi:10.3390/atmos12020235, 2021
- 604 Bonacci, O. (2010): Analysis of mean annual temperature series in Croatia, *Grđevinar*, 62(9), 781-791,
605 <https://hrcak.srce.hr/59611>, 2010
- 606 Bonacci, O.: Relationship between sea surface temperature (SST) and surface air temperature (SAT) along the eastern
607 Adriatic coast of Croatia, *Vodoprivreda*, 55, 325/326; 167-183, 2023
- 608 Duynkerke, P.G.: Radiation fog: A comparison of model simulation with detailed observations, *Mon. Weather Rev.*
609 119(2), 324-341, doi:10.1175/1520-0493(1991)119<0324:RFACOM>2.0.CO;2, 1991
- 610 Džoić, T., Zorica, B., Matić, F., Šestanović, M., Čikeš Keč, V.: Cataloguing environmental influences on the
611 spatiotemporal variability of Adriatic anchovy early life stages in the eastern Adriatic Sea using an artificial neural
612 network, *Front. Mar. Sci.* 9, 997937, doi:10.3389/fmars.2022.997937, 2022
- 613 Filonczuk, M.K., Cayan, D.R., Riddle, L.G.: Variability of marine fog along the California coast, *Scripps Institution*
614 *of Oceanography Report* 95-2, 102 pp., 1995
- 615 Fritzke, B.: A growing neural gas network learns topologies, *Adv. Neural Inf. Process. Syst.* 7, 625-632, 1995
- 616 Gultepe, I., Milbrandt, J.A.: Microphysical observations and mesoscale model simulation of a warm fog case during
617 FRAM project, *Pure Appl. Geophys* 164, 1161-1178, doi:10.1007/978-3-7643-8419-7_4, 2007

618 Gultepe, I., Tardif, R., Michaelides, S.C., Cermak, I., Bott, A., Bendix, J., Müller, M.D., Pagowski, M., Hansen, B.,
619 Ellrod, G., Jacobs, W., Toth, S., Cober, S.G.: Fog research: a review of past achievements and future perspectives,
620 *Pure and Appl. Geophys.* 164(6-7), 1121-1159, doi:10.1007/s00024-007-0211-x, 2007

621 Hersbach, H.; Bell, B.; Berrisford, P.; Hirahara, S.; Horányi, A.; Muñoz-Sabater, J.; Nicolas, J.; Peubey, C.; Radu, R.;
622 Schepers, D.; Simmons, A.; Soci, C.; Abdalla, S.; Abellan, X.; Balsamo, G.; Bechtold, P.; Biavati, G.; Bidlot, J.;
623 Bonavita, M.; De Chiara, G.; Dahlgren, P.; Dee, D.; Diamantakis, M.; Dragani, R.; Flemming, J.; Forbes, R.; Fuentes,
624 M.; Geer, A.; Haimberger, L.; Healy, S.; Hogan, R. J.; Hólm, E.; Janisková, M.; Keeley, S.; Laloyaux, P.; Lopez, P.;
625 Lupu, C.; Radnoti, G.; de Rosnay, P.; Rozum, I.; Vamborg, F.; Villaume, S.; Thépaut, J.-N. (2020a): The ERA5 global
626 reanalysis, *Q. J. R. Meteorol. Soc.* 146, 1999–2049, doi:10.1002/qj.3803, 2020

627 Hersbach, H.; Bell, B.; Berrisford, P.; Hirahara, S.; Horányi, A.; Muñoz-Sabater, J.; Nicolas, J.; Peubey, C.; Radu, R.;
628 Schepers, D.; Simmons, A.; Soci, C.; Abdalla, S.; Abellan, X.; Balsamo, G.; Bechtold, P.; Biavati, G.; Bidlot, J.;
629 Bonavita, M.; De Chiara, G.; Dahlgren, P.; Dee, D.; Diamantakis, M.; Dragani, R.; Flemming, J.; Forbes, R.; Fuentes,
630 M.; Geer, A.; Haimberger, L.; Healy, S.; Hogan, R. J.; Hólm, E.; Janisková, M.; Keeley, S.; Laloyaux, P.; Lopez, P.;
631 Lupu, C.; Radnoti, G.; de Rosnay, P.; Rozum, I.; Vamborg, F.; Villaume, S.; Thépaut, J.-N. (2020b): ERA5 hourly
632 data on pressure levels from 1979 to present, Copernicus Climate Change Service (C3S) Climate Data Store (CDS),
633 doi:10.1002/qj.3803, 2020

634 Huang, B., Zhang, J., Cao, Y., Gao, X., Ma, S., Sun, C.: Improvements of sea fog forecasting based on CMA-TYM,
635 *Front. Earth Sci.* 10: 854438, doi: 10.1016/j.jastp.2022.105958, 2022

636 Ju, T., Wu, B., Zhang, H., Liu, J.: Parameterization of radiation fog-top height and methods evaluation in Tianjin,
637 *Atmosphere* 11(5), 480, doi:10.3390/atmos11050480, 2020

638 Kawai, H., Koshiro, T., Endo, H., Arakawa, O., Hagihara, Y., Changes in marine fog in a warmer climate., *Atmos.*
639 *Sci. Lett.* 17, 548-555, doi:10.1002/asl.691

640 Klaić Z. B., Pasarić Z., Tudor M.: On the interplay between sea-land breezes and etesian winds over the Adriatic, *J.*
641 *Mar. Sys.* 78, 101–118, doi: 10.1016/j.jmarsys.2009.01.016, 2009

642 Klemm, O., Lin, N.: What causes observed fog trends: air quality or climate change? *Aerosol. Air. Qual. Res.* 16,
643 1131-1142, doi:10.4209/aaqr.2015.05.0353

644 Koračin, D., and Dorman, C.E. (Eds): *Marine fog: challenges and advancements in observations and forecasting*,
645 Springer Atmospheric Sciences Series, Springer International Publishing, Cham, Switzerland, 537 pp.,
646 doi:10.1007/978-3-319-45229-6_7, ISBN 978-3-319-45227-2, 2017

647 Koračin, D., Lewis, J., Thompson, W.T., Dorman, C.E., Businger, J.A.: Transition of stratus into fog along the
648 California coast: observations and modeling, *J. Atmos. Sci.* 58, 1714-1731, doi:10.1175/1520-
649 0469(2001)058%3C1714:TOSIFA%3E2.0.CO;2, 2001

650 Kulkarni, R., Jenamani, R.K., Pithani, P., Konwar, M., Nigam, N., Ghude, S.D.: Loss to aviation economy due to
651 winter fog in New Delhi during the winter of 2011-2016, *Atmosphere*, 10(4), 198, doi:10.3390/atmos10040198, 2019

652 Li, G., Cheng, L., Zhu, J., Trenberth, K.: Increasing ocean stratification over the past half-century, *Nat. Clim. Change*
653 10(12), 1-8, doi:10.1038/s41558-020-00918-2, 2020

654 Mariani, L.: Fog in the Po valley: Some meteo-climatic aspects, *Ital. J. Agrometeorol.* 3: 35-44, 2009

655 Martinetz, T., Schulten, K.: A “neural-gas” network learns topologies, in: Proceedings of the International Conference
656 on Artificial Neural Networks 1991, 397-402, 1991

657 Matić, F., Džoić, T., Kalinić, H., Čatipović, L., Udovičić, D., Juretić, T., Rakuljić, L., Sršen, D., Tičina, V.:
658 Observation of abrupt changes in the sea surface layer of the Adriatic Sea, *J. Mar. Sci. Eng.* 10, 848,
659 doi:10.3390/jmse10070848, 2022

660 Merchant, C. J.; Embury, O.; Bulgin, C. E.; Block, T.; Corlett, G. K.; Fiedler, E.; Good, S. A.; Mittaz, J.; Rayner, N.
661 A.; Berry, D.; Eastwood, S.; Taylor, M.; Tsushima, Y.; Waterfall, A.; Wilson, R.; Donlon, C.: Satellite-based time-
662 series of sea-surface temperature since 1981 for climate applications, *Sci Data* 6(1) 1-18, doi: 10.1038/s41597-019-
663 0236-x, 2019

664 Omazić, B., Telišman Prtenjak, M., Prša, I., Belušić Vozila, A., Vučetić, V., Karoglan, M., Karoglan Kontić, J., Prša,
665 Ž., Anić, M., Šimon, S., Güttler, I.: Climate change impacts on viticulture in Croatia; viticultural zoning and future
666 potential, *Int. J. Climatol.* 40, 5634 – 5655, doi:10.1002/joc.6541, 2020

667 Oztaner, Y.B., Yilmaz, A.: An examination of fog and PM10 Relationship for Ataturk and Esenboga International
668 Airports of Turkey, in: Proceedings of the 6th Atmospheric Science Symposium - ATMOS 2013, Istanbul Technical
669 University, 2013

670 Pandžić K., Likso T.: Eastern Adriatic typical wind field patterns and large-scale atmospheric conditions, *Int. J.*
671 *Climatol.* 25, 81–98, doi:10.1002/joc.1085, 2005

672 Pastor, F., Valiente, J.A., Palau, J.L.: Sea surface temperature in the Mediterranean: trends and spatial patterns, *Pure*
673 *and Appl. Geophys.* 175, 4017-4029, doi:10.1007/s00024-017-1739-z, 2018

674 Pawlowicz, R.: M_Map: A mapping package for MATLAB, version 1.4m, [Computer software], available online at
675 www.eoas.ubc.ca/~rich/map.html, 2020

676 Popović, R., Kulović, M., Stanivuk, T.: Meteorological safety of entering eastern Adriatic ports, *Trans. Marit. Sci.*
677 2014 (1), 53-60, doi:10.7225/toms.v03.n01.006, 2014

678 Stipaničić, V.: Fog on the western coast of the Istria peninsula, *Vijesti Pomorske meteorološke službe*, 18, 7-10,
679 <https://library.foi.hr/dbook/cas.php?B=1&item=S02101&godina=1972&broj=00001>, 1972

680 Stolaki, S.N., Kazadzis, S.A., Foris, D.V., Karacostas, Th.S.: Fog characteristics at the airport of Thessaloniki, Greece,
681 *Nat. Hazards Earth Syst. Sci.* 9: 1541-1549, doi:10.5194/nhess-9-1541-2009, 2009

682 Šantić, D., Piwosz, K., Matić, F., Vrdoljak Tomaš, A., Arapov, J., Dean, J. L., Šolić, M., Koblížek, M., Kušpilić, G.,
683 Šestanović, S.: Artificial neural network analysis of microbial diversity in the central and southern Adriatic Sea, *Sci.*
684 *Rep.* 11, 1–15, doi:10.1038/s41598-021-90863-7, 2021

685 Šimunić, I., Likso, T., Husnjak, S., Bubalo Kovačić, M.: Analysis of climate elements in central and western Istria for
686 the purpose of determining irrigation requirements of agricultural crops, *Agric. Conspec. Sci.* 86(3), 225-233,
687 <https://hrcak.srce.hr/file/382381>, 2021

688 Tardif, R., Rasmussen, R.M.: Event-based climatology and typology of fog in the New York City region, *J. App.*
689 *Meteorol. Climatol.*, 46, 1141-1168, doi:10.1175/JAM2516.1, 2007

690 Telišman Prtenjak, M., Grisogono, B.: Sea-land breeze climatological characteristics along the northern Croatian
691 Adriatic coast, *Theor. Appl. Climatol.* 90, 201–215, doi:10.1007/s00704-006-0286-9, 2007

692 Telišman Prtenjak, M., Viher, M., Jurković, J.: Sea-land breeze development during a summer bora event along the
693 north-eastern Adriatic coast, *Q. J. Roy. Meteorol. Soc.* 136, 1554–1571, doi:10.1002/qj.649, 2010
694 Tešić, M., Brozinčević, K.: Fog phenomenon on the eastern coast of the Adriatic Sea, *Hydrografski godišnjak* 1974,
695 91-116, 1974
696 Tojčić, I., Denamiel, C., Vilibić, I.: Kilometer-scale trends and variability of the Adriatic present climate, (1987–
697 2017), *Clim. Dyn* 61, 2521–2545, 10.1007/s00382-023-06700-2
698 Tojčić, I., Denamiel, C., Vilibić, I.: Kilometer-scale trends, variability, and extremes of the Adriatic far-future climate
699 (RCP 8.5, 2070-2100), *Front. Mar. sci.* 16, 907–926, doi:10.3389/fmars.2024.1329020, 2024
700 Vautard, R., Yiou, P., van Oldenborgh, G.: The decline of fog, mist and haze in Europe during the last 30 years, *Nat.*
701 *Geosci.* 2, 115–119, doi:10.1038/ngeo414, 2009
702 Veljović, K., Vujović, D., Lazić, L.: An analysis of fog events at Belgrade International Airport, *Theor. Appl.*
703 *Climatol.* 119 (1-2), 13-24, doi:10.1007/s00704-014-1090-6, 2015
704 WMO, *International Meteorological Vocabulary*, World Meteorological Organization, Geneva, Switzerland, pp. 141.,
705 1966
706 Wang, Y., Niu, S. J., Lv, J. J., Lu, C. S., Xu, X. Q., Wang, Y. Y., Ding, J., Zhang, H., Wang, T., Kang, B.: A new
707 method for distinguishing unactivated particles in cloud condensation nuclei measurements: implications for aerosol
708 indirect effect evaluation, *Geophys. Res. Lett.* 46, 14185–14194, doi:10.1029/2019gl085379, 2019
709 Zoldoš, M., Jurković, J.: Fog event climatology for Zagreb Airport, *Croatian Met. Journal* 51(51), 13-26,
710 <https://hrcak.srce.hr/168218>, 2016